ACS APPLIED MATERIALS & INTERFACES

Research Article

www.acsami.org

Self-Assembled Hierarchical Formation of Conjugated 3D Cobalt Oxide Nanobead−CNT−Graphene Nanostructure Using Microwaves for High-Performance Supercapacitor Electrode

Rajesh Kumar,*[,†] Rajesh Kumar Singh,*[,‡] Pawan Kumar Dubey,[§] Dinesh Pratap Singh,[∥] and Ram Manohar Yadav[⊥]

[†]Center for Semiconductor Components, State University of Campinas (UNICAMP), 13083-870 Campinas, Sao Paulo, Brazil

[‡]Department of Physics, Indian Institute of Technology (Banaras Hindu University), Varanasi 221005, India

[§]Nanotechnology Application Centre, University of Allahabad, Allahabad 211002, India

[∥]Departamento de Física, Universidad de Santiago de Chile, Avenida Ecuador 3493, Estacíon Central, Santiago 9170124, Chile

[⊥]Department of Physics, VSSD College, Kanpur 208002, India

ABSTRACT: Here we report the electrochemical performance of a interesting three-dimensional (3D) structures comprised of zero-dimensional (0D) cobalt oxide nanobeads, one-dimensional (1D) carbon nanotubes and two-dimensional (2D) graphene, stacked hierarchically. We have synthesized 3D self-assembled hierarchical nanostructure comprised of cobalt oxide nanobeads (Co-nb), carbon nanotubes (CNTs), and graphene nanosheets (GNSs) for high-performance supercapacitor electrode application. This 3D self-assembled hierarchical nanostructure Co_3O_4 nanobeads−CNTs−GNSs (3D:Co-nb@CG) is grown at a large scale (gram) through simple, facile, and ultrafast microwave irradiation (MWI). In 3D:Co-nb@CG nanostructure, Co_3O_4 nanobeads are attached to the CNT surfaces grown on GNSs. Our ultrafast, one-step approach not only renders simultaneous growth of cobalt oxide and CNTs on graphene nanosheets but also institutes the intrinsic dispersion of carbon nanotubes and cobalt oxide within a highly conductive scaffold. The 3D:Co-nb@CG electrode shows better electrochemical performance with a maximum specific capacitance of 600 F/g at the charge/discharge current density of 0.7A/g in KOH electrolyte, which is 1.56 times higher than that of Co_3O_4-decorated graphene (Co-np@G) nanostructure. This electrode also shows a long cyclic life, excellent rate capability, and high specific capacitance. It also shows high stability after few cycles (550 cycles) and exhibits high capacitance retention behavior. It was observed that the supercapacitor retained 94.5% of its initial capacitance even after 5000 cycles, indicating its excellent cyclic stability. The synergistic effect of the 3D:Co-nb@CG appears to contribute to the enhanced electrochemical performances.

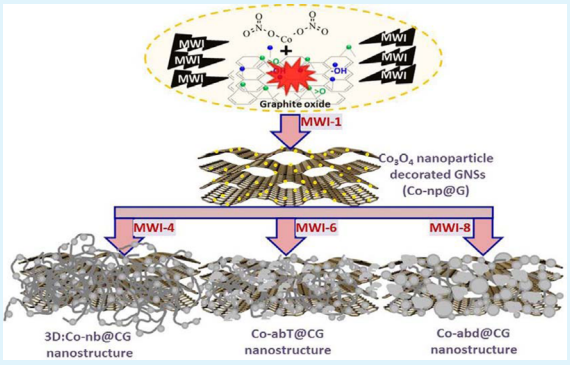

KEYWORDS: *graphene, CNT, cobalt oxide, supercapacitor, self-assembly, hierarchical nanostructures, nanobeads*

1. INTRODUCTION

The unique three-dimensional (3D) functional nanostructures based on two-dimensional (2D) carbon-based material, such as graphene nanosheets (GNSs), as the substrate for growth of one-dimensional (1D) carbon nanotubes (CNTs) have recently attracted attention due to their high surface-to-volume ratio arising from unique and new morphology. The 2D GNSs have several advantageous applications as high electrical conductor, solar cells,[1] batteries,[2] detector of polluting agents,[3] micro-supercapacitors,[4] transparent conductive films,[5] super hydrophobic surfaces, and so on. As we know, transition metal oxide nanostructures with GNS and CNT nanostructures show excellent electrochemical properties, leading to a number of interesting robust applications. Among all the transition metal oxide nanoparticles, cobalt oxide (Co_3O_4) nanoparticles play an important role as catalytic materials, ionic exchangers, and magnetic materials, as well as electrode materials with GNSs and CNTs. In addition, nanocomposites of Co_3O_4 with CNTs,[6] carbon nanofibers (CNFs),[7] GNSs,[8] and conducting polymers[9] have also been fabricated. These 3D GNS−CNT nanohybrid structures can be synthesized using microwave irradiation (MWI) method, which is one of the prominent thermochemical method, since in 3D nanostructure formation, the decomposition reaction mechanism is responsible.[10−12] MWI is an excellent technique for the synthesis of 3D carbon nanostructures using 1D and 2D carbon nano materials at high temperature. The MWI can heat the material in-depth quickly and uniformly, minimizing thermal gradients and reducing

Received: May 19, 2015
Accepted: June 18, 2015
Published: June 18, 2015

DOI: 10.1021/acsami.5b04336
ACS Appl. Mater. Interfaces 2015, 7, 15042−15051

diffusion time for the particles. Therefore, the reaction products are produced in a very short time as compared to others methods.[13−15] The reaction rates are influenced by the MWI applied power (W), the reaction time (t) and temperature (T) for the exposed sample. The final quality of the microwave-generated materials depends on the reactant choice, applied power, reaction time, and temperature. The use of MWI is readily scalable to larger reaction volumes, allows faster reaction times, removes the need for high-temperature injection, and suggests a specific microwave effect. There are some reports on combinations of 1D and 2D nanostructures such as graphene−SiO_2 nanorods,[16] graphene−metal nanorods,[17] graphene−CNTs,[18−20] and graphene−metal oxide[21,22] to produce heterogeneous 3D array structures. MWI methodology is unique in their ability to be scaled up, providing a potentially industrially important improvement in 3D carbon-based nanostructure over conventional methods. Synthesis of high-quality, nearly monodispersed nanostructures can be prepared via direct MWI heating of the molecular precursors rather than convective heating of the solvent. MWI heating not only enhances the rate of formation; it also enhances the material quality and reduces size inhomogeneity.

Here, we report a simple MWI based technique to synthesize 3D:Co-nb@CG nanostructures showing 0D-Co_3O_4 nanobeads attached to 1D carbon nanotubes, grown on 2D GNSs to produce heterogeneous 3D nanoarrays. The microwave-assisted method is employed to achieve this architecture because it offers great advantages such as faster synthesis and higher energy efficiency compared to other conventional methods.[23] This nanostructure has been synthesized in situ MWI method in which cobalt[24] nanoparticles act as a catalyst for the growth of CNTs on GNSs after that Co_3O_4 nanobeads are attached on the CNT surfaces. The Co nanoparticle reacts with GNSs at high temperature and absorbs the carbon species from GNSs and start to segregate in form of CNTs. This 3D:Co-nb@CG nanostructure has been used for supercapacitor electrode and it shows electric double layer capacitance (EDLC) behavior with high specific capacitance and stability.

2. EXPERIMENTAL SECTION

2.1. Synthesis of Graphite Oxide. The starting graphite oxide material was synthesized by the slightly modified Staudenmaiers method.[25] In a typical experiment, graphite powder (size, ∼40 μm; 10 g) was reacted with strong oxidizing solution of concentrated nitric and sulfuric acid (1:3 v/v). After 1 h of continuous magnetic stirring, this solution-containing flask was placed into an ice bath, and 90 g of potassium chlorate ($KClO_3$, 99%) was slowly added to this solution to avoid the formation of explosive chlorine gas. The whole solution was magnetically stirred for 5 days to avoid agglomeration and to obtain a homogeneous dispersion in solution. The as-obtained graphite oxide solution was washed several times with deionized (DI) water and 10% hydrochloric acid (HCl) solution to remove sulfate ions (SO_4^{2-}) and other ion impurities. The washed graphite oxide powder was dried at 40 °C in oven for 12 h. The as-prepared graphite oxide powder was a brownish powder and used for next step (for the synthesis of 3D:Co-nb@CG nanostructure).

2.2. MWI Synthesis of 3D:Co-nb@CG Nanostructure. In a typical synthesis route for 3D:Co-nb@CG, graphite oxide (30 mg) and cobalt nitrate ($Co(NO_3)_2{\cdot}6H_2O$) (0.7 mg, which was optimized after several experiments) were added to 65 mL of DI water, and then the solution was horn sonicated for 1.5 h and stirred for 30 min using magnetic stirrer for homogenization, respectively. Finally, this solution was dried in air at 50 °C overnight for complete evaporation of DI water. After that, this dried mixture powder was equally divided into five parts (∼6.0 mg) for MWI for different time. MWI was carried out in a domestic microwave oven, and each part was put into the microwave oven working at 2.45 GHz and a fixed power level of 800 W. The MWI reaction time was different for each sample (1, 2, 4, 6, and 8 min) for the formation of different nanostructures. The best 3D:Co-nb@CG structure was obtained with 4 min of microwave irradiation. During MWI, samples suddenly burned in the form of plasma and converted into black, highly porous materials with high surface area. The final different time irradiated samples were used for the characterization.

2.3. Materials Characterization. The as-synthesized materials were characterized by X-ray diffraction (XRD, Rigaku D/max-2550 V, Cu-Kα radiation). The sample was scanned for 2θ from 5.0 to 80°. The shape and morphology of the as-obtained 3D:Co-nb@CG materials were characterized by Nova NanoSEM 230 FEI at 5 kV in gentle-beam mode without any metal coating with the fully dried sample loaded on a carbon tape. The X-ray photoelectron spectroscopy (XPS) spectrum was recorded on a MultiLab2000 photoelectron spectrometer (Thermo-VG Scientific, Waltham, MA) with Al-Kα (1486.6 eV) as the X-ray source. All XPS spectra were corrected using the C 1s line at 284.6 eV. The transmission electron microscopy (TEM) analysis was carried out using JEM-3011HR microscope operating at 200 kV using a holey carbon-coated copper grid. The sample was prepared by dispersing a small amount of dry powder in ethanol or water. Then, one droplet of the suspension was dropped on a holey-carbon coated, 300 mesh copper TEM grids and allowed to dry in air at room temperature. The Raman spectrum was recorded on a LabRAM HR UV/vis/NIR (Horiba JobinYvon, France) using a CW Ar-ion laser (514.5 nm) as an excitation source focused through a confocal microscope (BXFM, Olympus, Japan) equipped with an objective lens (50 μm, numerical aperture 0.50) at room temperature. The changes in the surface chemical bonding and surface composition were characterized by Fourier transform infrared spectroscopy (FT-IR, Jasco FT-IR 4100). The test samples were pressed into tablets with KBr.

2.4. Preparation of Electrode and Electrochemical Measurement. The super capacitor electrodes were made separately from the 3D:Co-nb@CG, Co-np@G and agglomerated Co_3O_4 beads with CNTs lying on the GNSs surfaces (Co-abd@CG) nanostructure materials, mixed with 5 wt % nafion binder, with a porous polypropylene film as the separator and 30 wt % KOH aqueous solution as the electrolyte. The mixture of 3D:Co-nb@CG nanostructure and the binder was homogenized in C_2H_5OH in ultrasonic bath for 20 min and subsequently dried for 10 h in a vacuum oven at 120 °C (for complete removal of liquids). The as-prepared electrodes were pressed on a nickel (Ni) foam current collecting electrode with a bench press at a pressure of 20 MPa and sandwiched in a stainless steel cell with a pressure of 160 MPa. The Ni-foam-coated nanostructured materials served as the working electrode, and a platinum electrode and a Ag/AgCl electrode served as counter and reference electrodes, respectively. Electrochemical measurements, such as cyclic voltammetry (CV) and galvanostatic charge/discharge were carried out by a VersaSTAT 3 (Princeton Applied research). CV tests were performed between 0 and 1.2 V at 60 mV/s scan rate. Galvanostatic charge/discharge curves were measured in the potential range of 0 to 1.2 V (vs Ag/AgCl) between 0.7 and 4.5 A/g.

3. RESULTS AND DISCUSSION

3.1. Characterization of 3D:Co-nb@CG Nanostructure. The surface morphology of the products was analyzed using scanning electron microscopy (SEM). Figure 1 shows the SEM images of the as-synthesized 4 min microwave irradiated material (MWI-4). This reaction time provides sufficient temperature for nucleation and growth of CNTs and Co_3O_4 nanobeads. A large number of CNTs with diameters of 10−50 nm and length in microns, anchored with Co_3O_4 nanobeads were grown on graphene nanosheets, termed 3D:Co-nb@CG, are shown in Figure 1b−d. The Co_3O_4 nanobeads and nanoparticles having diameters of 200−250 nm were beaded

DOI: 10.1021/acsami.5b04336
ACS Appl. Mater. Interfaces 2015, 7, 15042−15051

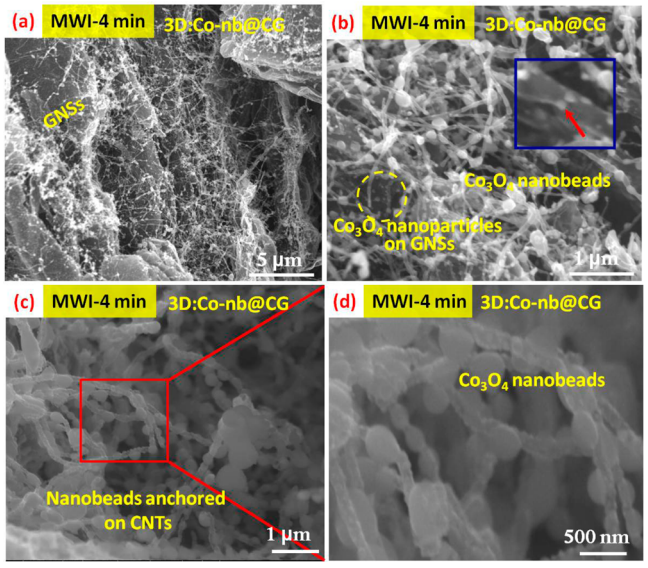

Figure 1. SEM images of the MWI reaction time for 4 min and formation of 3G:Co-nb@CG nanostructure at (a−c) low magnification and (d) high magnification.

on the CNTs like a necklace (Figure 1b,c) and the length of CNTs on the graphene sheets in nearly 8−10 nm. It is also noteworthy that a significant portion of Co_3O_4 nanoparticles are imbedded within GNSs layers, as marked in the inset of Figure 1b. Such a geometric confinement of metal oxide within graphene has improved their interfacial contact, suppressed the agglomeration of nanobeads, and remarkably enhanced the electrochemical activity.[26] This MWI-4 condition was the optimum growth condition for the formation of 3D:Co-nb@CG nanostructure. Nanobead structures in long chain units were found everywhere over the entire CNT, as evidenced from Figure 1d. This gives evidence for a high degree of transformation of Co_3O_4 nanoparticles into Co_3O_4 nanobead-like structures.

MWI was also conducted for 1, 2, 6, and 8 min, but the best structures of 3D:Co-nb@CG nanostructure were achieved with MWI-4. Figure 2a shows the SEM micrograph of the sample treated with microwave for 1 min (MWI-1). As can be seen from this image, the Co_3O_4 nanoparticles are decorated on GNSs (Co-np@G) with no evidence of CNT growth. It seems that the MWI-1 condition is not sufficient enough for the nucleation and growth of nanobeads or CNTs on GNSs, and that is why only Co_3O_4 nanoparticles are decorated on the GNSs with the help of functional (epoxy, hydroxyl, carbocyclic, and carboxyl on its surface and edges) group attached on the GNSs surfaces. Figure 2b shows the microstructure of the 2 min (MWI-2) microwave-treated sample in which CNTs start to grow on the GNSs surface and Co_3O_4 nanoparticles are present on the GNSs surfaces (Co-np@CG). These CNTs have smaller lengths, as they appear on the GNSs, because the reaction time of 2 min MWI was not long enough to provide the sufficient temperature for the complete growth of nanobeads or longer CNTs. It is believed that as-grown CNTs originated from the GNSs, which acted as a carbon source for the formation of CNTs, because we did not provide any external carbon source for the growth of CNTs.

Figure 2c shows the SEM image of MWI reaction time for 6 min (MWI-6). This shows that the higher MWI reaction time affected the size of Co_3O_4 nanobeads due to high energy; these nanobeads started to melt and agglomerate (Co-ab). These agglomerated nanobeads attached on the CNTs have larger diameter as compared to MWI-4 (Figure 1d). Nanobead size increased because of the agglomeration, and CNTs were not able to lift them from the GNSs. It can be clearly seen in the

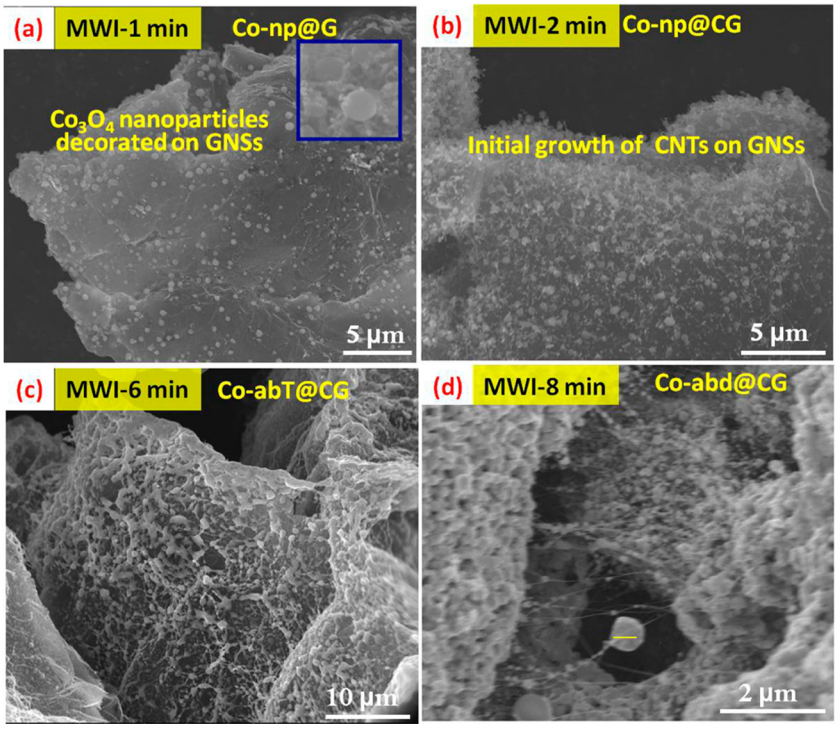

Figure 2. SEM images of the MWI for different reaction times and formation of different heterostructures: (a) Co-np@G, (b) Co-nb@CG, (c) Co-abT@CG, and (d) Co-abd@CG nanostructures.

DOI: 10.1021/acsami.5b04336
ACS Appl. Mater. Interfaces 2015, 7, 15042−15051

Table 1. SEM Microstructural Observation and Description for Different MWI Reaction Time for Different Nanostructure

serial no.	nanostructure formation	MWI time (min)	structure formation	CNT formation and its observation
1	Co-np@G	1 (MWI-1)	Co_3O_4 nanoparticles are decorated on GNSs	no evidence of CNTs, and Co_3O_4 nanoparticles are uniformly distributed on graphene sheets
2	Co-np@CG	2 (MWI-2)	CNTs start to grow on the GNSs surfaces, and Co_3O_4 nanoparticles are present on the GNSs surfaces	CNTs start to grow on graphene surfaces with nanobeads
3	3D:Co-nb@CG	4 (MWI-4)	3D Co_3O_4 nanobeads anchored on CNTs and grown on GNS surfaces	CNTs grown very well with anchored Co_3O_4 nanobeads
4	Co-abT@CG	6 (MWI-6)	agglomerated Co_3O_4 beads with CNTs tangentially lying on the GNSs surfaces	CNTs tangentially lying on the GNSs surfaces
5	Co-abd@CG	8 (MWI-8)	agglomerated Co_3O_4 beads with CNTs lying on the GNSs surfaces	CNTs covered by agglomerated Co_3O_4 nanobeads

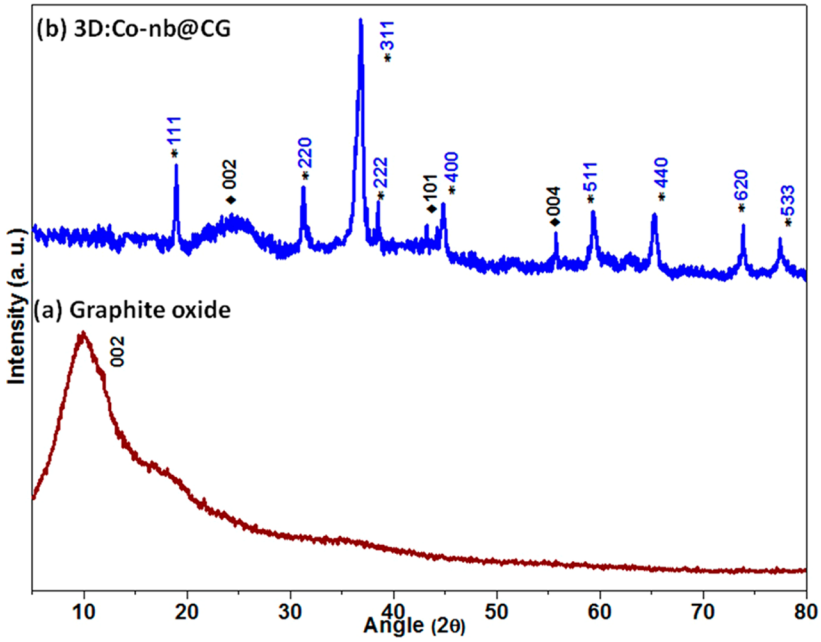

Figure 3. XRD pattern of as synthesized (a) graphite oxide and (b) 3D:Co-nb@CG nanostructure.

form of agglomerated beads tangentially lying on the GNSs (Co-abT@CG: agglomerated beads tangentially aligned) due to the larger, overweight nanobeads. Figure 2d shows the MWI reaction time for 8 min (MWI-8), and it shows that maximum CNTs were covered by densely formed agglomerated nanobeads (Co-abd@CG) except few CNTs as observed in SEM image. There are few CNTs which contains Co_3O_4 nanobeads, and these nanobeads hang on GNSs. The 3D:Co-nb@CG nanostructure as obtained at MWI-4 condition is the best compared to those obtained at MWI-1, MWI-2, MWI-6, and MWI- 8 conditions. The detailed morphological description has been given in Table 1 for various MWI reaction times and related structures.

The phase purity and crystal structures were further analyzed by X-ray diffraction (XRD). Figure 3 shows an XRD pattern of the as-synthesized materials. Figure 3a shows the XRD pattern of graphite oxide. The peak at 2θ = 9.82° corresponds to the interlayer spacing defined by the (002) peak with a spacing of 8.6 Å. After MWI for 4 min (MWI-4), this (002) peak shifted to higher angle at 2θ = 24.7°, corresponding to a spacing of 3.43 Å in 3D:Co-nb@CG nanostructure, as shown in Figure 3b. The broadening of (002) peak of graphene in 3D:Co-nb@CG nanostructure reveals the low number of graphene layers. The well-resolved diffraction peaks in Figure 3b reveal the good crystallinity of the as-synthesized materials. The diffraction peaks identify the sample as a mixture of cubic Co_3O_4 (a = 8.0722 Å, JCPDS no. 43-1003) and carbon-based crystalline materials. The broadest peak reflection arising from the graphene−CNT hybrid nanostructures corresponds to the (002) line at ca. 2θ = 24.4°. CNTs represent few sharp and small diffraction peaks located at 2θ of 44.2 and 55° corresponding to (100) and (004) reflections, respectively. The crystallization peaks of the Co_3O_4 powder is formed at 2θ = 19.1, 31.2, 36.8, 45, 59.4, 65.3, 73.7, and 77.3, corresponding to the (111), (220), (311), (400), (511), (440), (620), and (533) reflections planes, respectively.[27,28] These results show spinel Co_3O_4 with high intensity, which indicates the formation of large particles. No obvious peaks corresponding to cobalt nitrate or cobalt hydrate were observed in the XRD pattern. The well-resolved diffraction peaks in Figure 3b reveal the good crystalline nature of Co_3O_4 nanobeads.

XPS was carried out to analyze the states of each element on the surface, nature of chemical bonding and stoichiometric composition. The survey spectra of 3D:Co-nb@CG nanostructure shows the presence of only C, Co, and O as shown in Figure 4a.[29] The wide survey XPS spectrum shows the predominant presence of carbon (84.6 at. %), oxygen (10.43 at. %), and cobalt (4.93 at. %). The atomic composition of the beaded Co_3O_4 reveals the presence of oxygen atoms in the cobalt oxide. The high-resolution Co 2p XPS spectra of the

DOI: 10.1021/acsami.5b04336
ACS Appl. Mater. Interfaces 2015, 7, 15042−15051

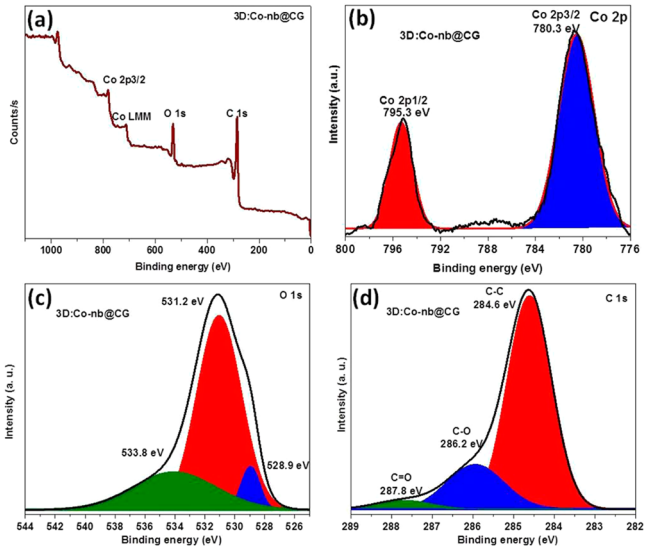

Figure 4. XPS spectra of (a) complete survey, (b) Co 2p, (c) O 1s, and (d) C 1s core level for 3D:Co-nb@CG nanostructure.

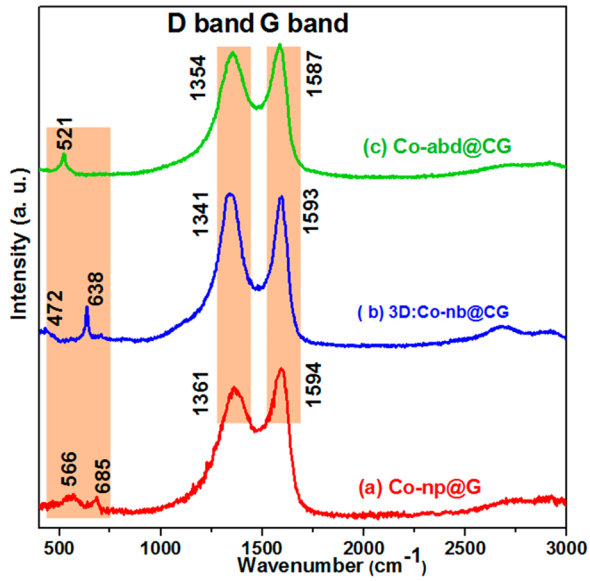

Figure 5. Raman spectra of (a) Co-np@G, (b) 3D:Co-nb@CG, and (c) Co-abd@CG nanostructure.

Co_3O_4 exhibited the peaks at 795.3 and 780.3 eV, corresponding to Co $2p_{1/2}$ and Co $2p_{3/2}$ peaks (Figure 4b). These two major peaks with binding energies at 795.3 and 780.3 eV correspond to Co $2p_{1/2}$ and Co $2p_{3/2}$, respectively, with a spin energy separation of 15.0 eV, which is the characteristic of a Co_3O_4 phase.[30] The complex Co 2p spectrum indicates the presence of two chemically distinct species: Co^{2+} and Co^{3+}. In addition, the presence of Co_3O_4 nanobeads could be further confirmed by O 1s XPS peak which could be deconvoluted into three peaks (Figure 4c). The peaks located at 531.2 and 533.8 are ascribed to oxygen atoms in the hydroxyl groups and absorbed water, respectively, while the peak at 528.9 eV is assigned to oxygen atoms in Co_3O_4.[31,32] The increased intensity of O 1s in the hydroxyl groups in 3D:Co-nb@CG nanostructure is contributed from the incorporation of functional group present on the GNSs surfaces. The C 1s spectrum (Figure 4d) shows a dominant peak centered at 284.6 eV with two weak peaks at 286.2 and 287.8 eV, as shown in Figure 4d. The C 1s peak at 284.6 eV is due to sp^2 C−C bonds. The weak peaks at approximately 286.2 and 287.8 eV correspond to C−O bonds in the epoxy/ether groups and C═O bonds in the ketone/carboxylic groups, respectively.

Notable differences can also be observed in Raman spectra, as shown in Figure 5. Raman spectra were employed to investigate the vibrational properties of Co-np@G, 3D:Co-nb@CG and Co-abd@CG nanostructures. Two distinct and sharp peaks were observed, for the D band and the G band for all MWI reaction time. This is commonly observed for all graphitic structures and can be attributed to the E_{2g} vibrational mode present in the sp^2 bonded graphitic carbons. The G band arises from the first-order scattering of the E1g phonon of sp^2 C atoms, while the D mode is a breathing mode of κ-point photons of A1g symmetry. Thus, the G band is the result of vibration of sp^2 C atoms and the D band arises from the disorder and defect intensity of the crystal structure.[33] The relative intensity ratio of D and G band (I_D/I_G) can be used to quantify the relative content of defects and the sp^2 domain size. The I_D/I_G for Co-np@G, 3D:Co-nb@CG and Co-abd@CG nanostructures is 0.89, 1.01, and 0.99 respectively. The I_D/I_G ratio and peak positions for Co-np@G, 3D:Co-nb@CG and Co-abd@CG nanostructures have been shown in Table 2. These ratio (I_D/I_G) confirms that 3D:Co-nb@CG have maximum disordered structure and Co-np@G have the minimum disordered structure. The result demonstrates that more defects have been introduced into the 3D:Co-nb@CG nanostructures due to the growth of CNTs on GNSs with Co_3O_4 nanobeads. We can see that D band in 3D:Co-nb@CG significantly upshifted compared to the Co-np@G and Co-abd@CG nanostructures which also give the evidence of more defected structure. Some weak peaks also appeared in Raman spectra toward lower wavelength side. These peaks correspond to $1E_g$ (472 cm^{-1}), $3F_{2g}$ (521, 566, and 638 cm^{-1}), and A_{1g} (685 cm^{-1}) for the Raman active modes of the Co_3O_4, respectively, of which the phonon symmetries are caused by the lattice vibrations of the spinel structure of Co_3O_4.[34,35] The phonon symmetries of the Raman peaks are caused by the lattice vibrations of the spinel structure, in which Co^{2+} and Co^{3+} cations are situated at tetrahedral and octahedral sites in the cubic lattice.

The presence of Co_3O_4 in Co-np@G, 3D:Co-nb@CG and Co-abd@CG were also confirmed by the FTIR analysis. The as-followed features of FTIR spectra can be found in Figure 6, a broad, intense band at around 3460 cm^{-1} correspond to O−H stretching vibrations. The other peaks at 1644, 1464, and 1256 cm^{-1} were attributed to the vibrations of C═C (stretching vibrations), O−H (bending vibrations from hydroxyl groups) and breathing vibrations from epoxy groups, respectively.[24,36] Additionally, the strong and sharp absorption peaks at 578 and 661 cm^{-1} are attributed to the vibration of the Co−O, confirming the existence of Co_3O_4 nanobeads in the as-synthesized sample.[37,38]

3.2. Electrochemical Performance and Responsible Mechanism. Graphene shows major applications in energy storage systems such as super capacitors and in lithium ion batteries, but as we know, that restacking of GNSs as demerit tendency of graphene and has a detrimental effect on the performance of graphene as electrode materials applications. To test the electrode efficiency of our 3D:Co-nb@CG nanostructure, we fabricated the coin cells with the two-electrode configuration. The electrodes were made of the 3D:Co-nb@

DOI: 10.1021/acsami.5b04336
ACS Appl. Mater. Interfaces 2015, 7, 15042−15051

Table 2. Raman Peak Positions of As-Synthesized Co-np@G, 3D:Co-nb@CG and Co-abd@CG Nanostructures

serial no.	nanostructure formation	Raman active modes		band position (cm^{-1})		I_D/I_G
		mode	position (cm^{-1})	D band	G band	
1	Co-np@G	F_{2g} and A_{1g}	566, 685	1361	1594	0.89
2	3D:Co-nb@CG	E_g and F_{2g}	472, 638	1341	1593	1.01
3	Co-abd@CG	F_{2g}	521	1354	1587	0.99

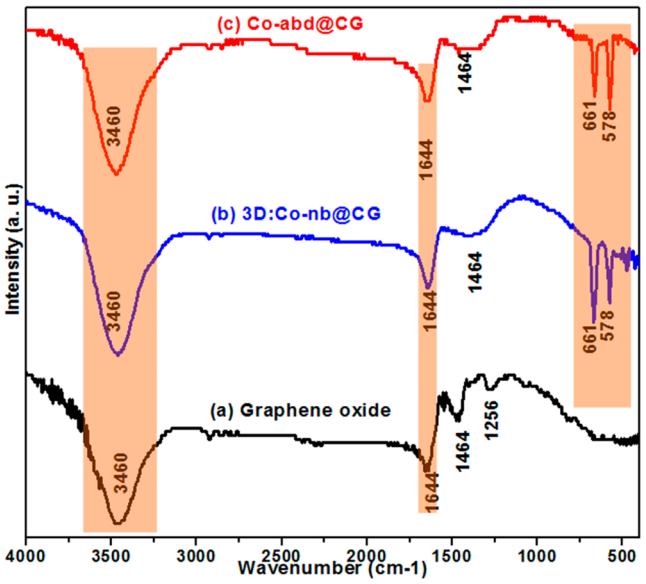

Figure 6. FTIR spectra of (a) graphene oxide, (b) 3D:Co-nb@CG, and (c) Co-abd@CG nanostructure.

CG nanostructure materials, mixed with 5 wt % Nafion binder, with a porous polypropylene film (as the separator) and tested in 30 wt % KOH aqueous solution as the electrolyte. The properties of super capacitors were investigated using cyclic voltametry (CV) and charge/discharge (DC) methods in the potential window of 0−1.2 V. Figure 7a, shows the CV curves of the super capacitors, the shapes of all the CV curves were nearly symmetrical rectangular, indicating an excellent super capacitive performance. In comparison, the CV curves of all the samples were measured under the same conditions at 60 mV/s (Figure 7a). The CV curves gradually deviate toward nearly rectangular shape as its area increases, indicating enhanced capacitive behavior of 3D:Co-nb@CG. Except 3D:Co-nb@CG, other both samples (Co-np@G and Co-abd@CG) consist of very broad redox peaks indicating the small contribution of pseudocapacitance to the total capacitance. One broad redox peaks appear between 0 and 0.5 V (vs Ag/AgCl), which is attributed to the faradaic reactions related to Co−O/Co−O−OH associated with −OH anions.[39]

The electrochemical performance of as-prepared electrodes was also evaluated by galvanostatic charge/discharge tests carried out under different current densities. The linear voltage−time curves in Figure 7b show a symmetric characteristic of charge/discharge curves indicating a good capacitive behavior of the high-performance supercapacitor electrode. The specific capacitance (Cs) of 3D:Co-nb@CG nanostructure calculated at 0.7, 1.1, 1.5, 1.9, 2.3, 2.7, 3.1, 3.5, 3.9, and 4.5 A/g from the discharge curves is found to be 600.19, 542.73, 509.85, 494.84, 489.87, 484.80, 480.78, 479.83, 479.00, and 478.93 F/g, respectively. These values are superior to those reported in previous studies for Co_3O_4@graphene nanocomposite (430 F/g, 1A/g),[40] graphene/Co_3O_4 composites (443 F/g, 5A/g),[41] rGO/Co_3O_4 hybrid (331 F/g, 5 A/g),[42] rGO-Co_3O_4 composite (416 F/g, 2 A/g)[43] and Co_3O_4/rGO composites (340 F/g, 1 A/g).[44] Figure 7b displays the relationship between Cs and charge/discharge current densities of Co-np@G, 3D:Co-nb@CG, and Co-abd@CG nanostructures. As expected, the capacitance decreases with an increase in current density due to limited diffusion on the electrode surface. Over the current density range of 2.0−4.5 A/g, all samples exhibit the stable specific capacitive performance. 3D:Co-nb@CG nanostructure shows that 79.79% specific capacitance was retained even with the current density increasing from 0.7 to 4.5 A/g. Additionally, the specific capacitance of other morphologies, such as Co-np@G (384.9F/g at 4.5 A/g), and Co-abd@CG (414.6 F/g at 4.5 A/g), have lower specific capacitance as compared to 3D:Co-nb@CG nanostructures. The specific capacitance of 3D:Co-nb@CG nanostructure is up to 600.19 F/g, is ∼1.56 times higher than Co-np@G nanostructure (384.9 F/g) with current density of 0.7 A/g. Consistent good performance of 3D:Co-nb@CG nanostructure over a wide range of current densities suggests this material as promising supercapacitor electrodes.

The improvement in specific capacitance and stability can probably be attributed to the unique structure of 3D:Co-nb@CG nanostructure. Attached Co_3O_4 nanobeads on CNTs surfaces and CNTs grown on GNSs surface provides a porous and highly conductive network for electron transport during the charge/discharge processes. The superior specific capacitance of 3D:Co-nb@CG nanostructure may be attributed to the synergetic effects between graphene and Co_3O_4 nanobeads attached on CNT in the novel 3D:Co-nb@CG nanostructure. First, GNSs as conductive substrate not only contributes in double-layer capacitance to the overall energy storage but also provides the efficient electron transfer channels for Co_3O_4 nanobeads. Second, the well-dispersed Co_3O_4 nanobeads on CNTs grown over GNSs can effectively prevent the stacking of GNSs to lead to available surface areas for the storage of charge. Third, the intimate interaction between the highly conductive GNSs with CNTs and Co_3O_4 nanobeads enables fast electron transport through the GNSs matrix to the Co_3O_4 nanobeads. Furthermore, the content of the Co_3O_4 nanobeads in the 3D:Co-nb@CG nanostructure plays an important role on their capacitance, which is related to their electronic resistance and pseudocapacitance. The 3D:Co-nb@CG nanostructure has lower charge transfer resistance than Co-np@G, owing to the fast ion diffusion and charge transfer of 3D:Co-nb@CG nanostructure. The excellent interfacial contact and increased contact area between Co_3O_4 nanobeads, CNTs, and GNSs can significantly improve the accessibility of 3D:Co-nb@CG nanostructure to the electrolyte ions and shorten the ion diffusion and migration pathways.

The stability of 3D:Co-nb@CG, Co-np@G, and Co-abd@CG nanostructures were evaluated by examination of 5000 galvanostatic charge/discharge between 0 and 1.2 V (vs Ag/AgCl) at a current density of 1.1 A/g (Figure 7d). The specific capacitance of the 3D:Co-nb@CG nanostructure electrode

DOI: 10.1021/acsami.5b04336
ACS Appl. Mater. Interfaces 2015, 7, 15042−15051

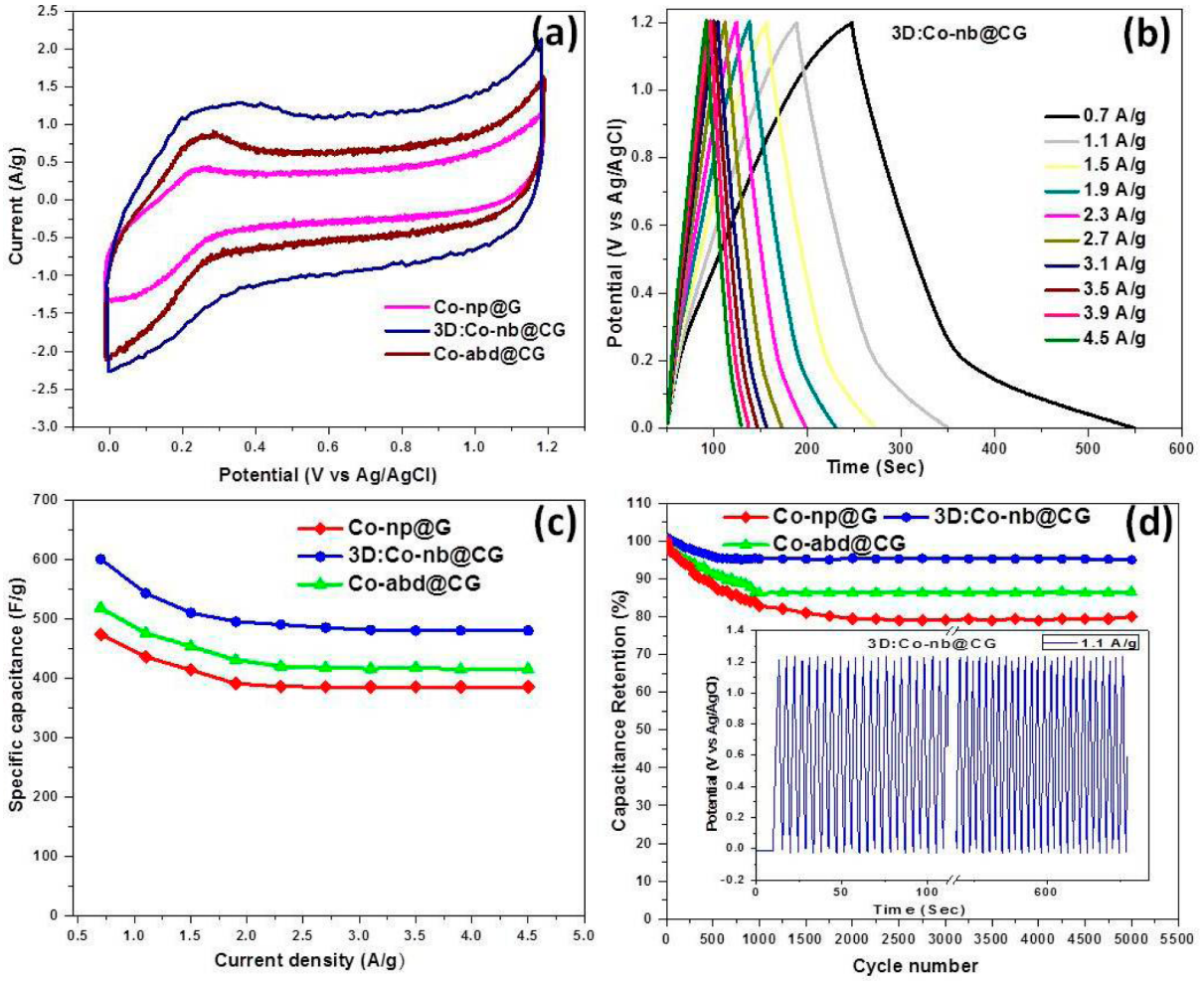

Figure 7. (a) CV curve for 3D:Co-nb@CG, Co-np@G, and Co-abd@CG nanostructure at 60 mV/s. (b) charge/discharge curves at different current densities for 3D:Co-nb@CG. (c) Specific capacitance of different nanostructure. (d) Capacitance retention of 3D:Co-nb@CG, Co-np@G, and Co-abd@CG nanostructure at 1.1 A/g; (inset) charge/discharge curve of electrochemical capacitor electrode obtained from 3D:Co-nb@CG at 1.1A/g.

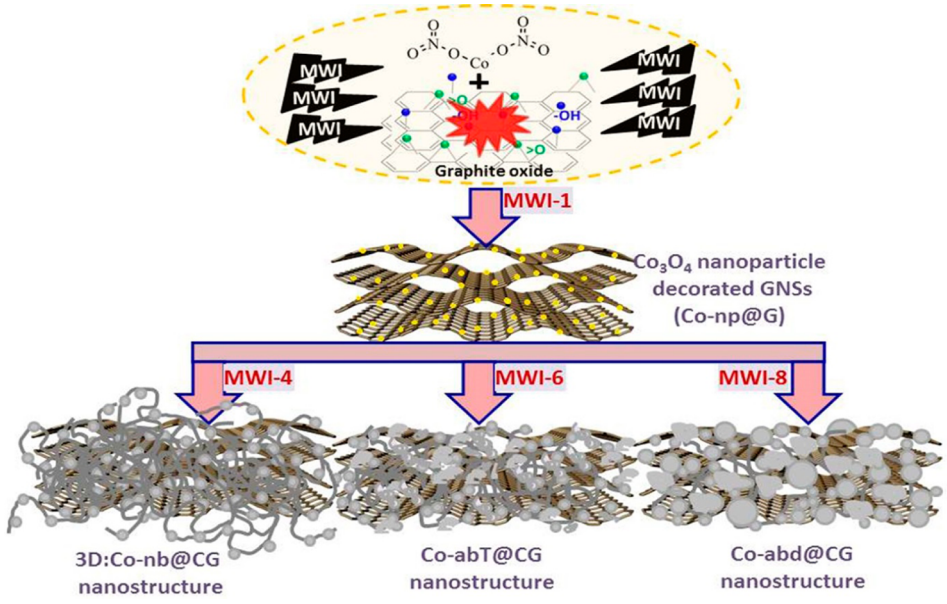

Figure 8. Mechanism for the growth and formation of 3D:Co-nb@CG nanostructures.

initially decreases during the first 550 cycles, and after that, it becomes stable due to the activation process in the super-capacitor electrode. The capacitance initially decreases 4.6% relative to the initial capacitance value until 550 cycles, and the

DOI: 10.1021/acsami.5b04336
ACS Appl. Mater. Interfaces 2015, 7, 15042−15051

capacitance is maintained without obvious aging or performance degradation, which demonstrates the excellent electrochemical performance of the 3D:Co-nb@CG nanostructure electrode material for application in practical energy storage devices. It is also observed that the supercapacitor retained 95.4% of its initial capacitance after 5000 cycles, indicating its excellent cycling stability. This nature of retention and long cycling stability shows good results in comparison to other previously reported for Co_3O_4@reduced graphene oxide nanoribbon (~94% capacitive retention after 2000 cycles).[45] The Co-np@G and Co-abd@CG nanostructure shows stable behavior until 1250 and 900 cycle, respectively, which is due to the unstable motion on Co_3O_4 nanoparticles on the GNSs and CNTs. The other electrodes such as Co-np@G and Co-abd@CG nanostructure have 16.4 and 7.7% less stability than 3D:Co-nb@CG nanostructure, respectively. The Co_3O_4 nanobeads are well attached to CNTs, the aggregation of Co_3O_4 nanobeads, and the cracking or crumbling of the electrode material during continuous cycling can be efficiently prevented. The 3D:Co-nb@CG nanostructure provides a path for the motion of electron in electrode materials. Furthermore, CNTs grown on GNSs can also serve as reliable conductive channels between individual active material components and current collectors. It is concluded that the synergistic effect between CNT-grown graphene sheets and Co_3O_4 nanobeads is responsible for the excellent electrochemical performance of the material.

3.3. Mechanism for the Formation of 3D:Co-nb@CG Nanostructure. The schematic diagram in Figure 8 shows the stepwise formation of the combined 1D and 2D nanostructure, which is highly dependent on the MWI reaction time. While the sample was irradiated in a microwave oven in the presence of air, the graphite oxide carbonaceous chemicals combusted and some gases blows out. In this process, a significant amount of heat might be released, and the local temperatures of the sample may be higher than the actual MWI temperature. During the MWI process, in situ thermal reduction of graphite oxide to GNSs and decomposition of cobalt nitrate ($Co(NO_3)_2{\cdot}6H_2O$) to Co ion nanoparticles occurs at same time during reaction processing. The Co nanoparticles catalyst plays a critical role in the formation of CNT on GNSs during the MWI process. It is known that graphene has some functional groups such as epoxy, hydroxyl, carbocyclic and carboxyl on its surface and edges that become negatively charged. The positive Co metal ions in the system would attach to and interact with the functional groups via electrostatic attraction and serve as nucleation precursors.[46] In our case, Co ions in this process would like to attach to some particular positions of the GNSs surfaces with functional group, and it shows the decoration of Co nanoparticles on GNSs surfaces as reaction time of MWI was for 1 min. At some higher MWI reaction time (2 min) the decorated Co nanoparticles act as catalyst for the growth of CNTs. As we know, that Co as transition metal has been used to employ to catalyze reactions involving carbon containing molecules. At longer MWI time (4 min), Co ions in this process would like to attach to some high density functional group containing surfaces of GNSs and then reduced to Co_3O_4 following MWI irradiation. This type of reduction ability has been reported in literature.[47,48] Also, we know that thermal decomposition of nitrate salts of some transition metals results the formations of metal oxides.[28,49,50] After the formation of Co_3O_4, these nanoparticles start to agglomerate and form nanobeads. As for the aggregation of Co_3O_4 nanoparticles, it has been proposed that the aggregation growth will initiate when the repulsive interactions among nanoparticles are not large enough to block their access due to van der Waals attraction.[51,52] The main driving force for oriented aggregation of Co_3O_4 nanoparticles is attributed to the tendency to decrease the high surface energy. These Co_3O_4 nanoparticles are spherical in structure, which minimizes their surface energy, and form nanobeads. During CNT growth, these Co_3O_4 nanobeads become well attached on the CNT outer surfaces and start to move in the growth direction and formation of 3D:Co-nb@CG nanostructure. At higher MWI reaction time (6 and 8 min), these nanobeads start to connect to each other because of high irradiation and show the agglomeration behavior and maximum CNTs has been covered by Co_3O_4 nanobeads. Although, these Co_3O_4 nanobeads show the unstable behavior and looks like bigger size Co_3O_4 nanoparticles and they deform the 3D:Co-nb@CG nanostructure.

Therefore, we can give a possible reaction mechanism for the growth of GNSs, CNTs, and Co_3O_4 nanobeads. The formation processes may be as

$$\text{graphite oxide} \rightarrow \text{GNSs} + \text{gases}$$

$$3Co(NO_3)_2{\cdot}6H_2O \rightarrow Co_3O_4 + 6NO_2 + 18H_2O + O_2$$

But, in practical the MWI is done on the mixed powder which contains graphite oxide and cobalt nitrate then combined reaction can be written as

$$\text{graphite oxide} + 3Co(NO_3)_2{\cdot}6H_2O \rightarrow \text{GNSs} + \text{CNTs} + Co_3O_4\text{nanobeads} + 6NO_2 + 18H_2O + O_2$$

4. CONCLUSION

In summary, we have developed a simple, ultrafast, facile, and inexpensive approach to fabricate self-assembled hierarchical 3D:Co-nb@CG nanostructures. This rapid and economical route (based on an efficient microwave-irradiation-assisted process) has been used to synthesize Co_3O_4 nanobeads containing CNTs on GNSs surface in large quantities. The unique structure of the 3D:Co-nb@CG, where CNTs, grown on GNSs and anchored by Co_3O_4 nanobeads, offer distinct advantages for energy storage as supercapacitors. These Co_3O_4 nanobeads discretely assembled along CNTs and form necklace-like structures. This unique morphological structure provides enhanced properties like high specific capacitance, long cycle ability, and stability. The synthesis route is an efficient, cost-effective, and potentially competitive approach for the formation of 3D hybrid nanostructures, which can be applied for the growth of electrodes for supercapacitors.

AUTHOR INFORMATION

Corresponding Authors

*E-mail: rajeshbhu1@gmail.com.
*E-mail: rksbhu@gmail.com.

Notes

The authors declare no competing financial interest.

ACKNOWLEDGMENTS

We would like to gratefully acknowledge anonymous referees for useful comments and constructive suggestions. D.P.S. acknowledges the support from Conicyt Fondecyt Regu-

DOI: 10.1021/acsami.5b04336
ACS Appl. Mater. Interfaces 2015, 7, 15042−15051

lar:1151527 Chile. R.K.S. and P.K.D. acknowledges the financial support from UGC, New Delhi.

REFERENCES

(1) Yang, L.; Yu, X.; Hu, W.; Wu, X.; Zhao, Y.; Yang, D. An 8.68% Efficiency Chemically-Doped-Free Graphene−Silicon Solar Cell Using Silver Nanowires Network Buried Contacts. *ACS Appl. Mater. Interfaces* **2015**, *7*, 4135−4141.

(2) Datta, D.; Li, J.; Shenoy, V. B. Defective Graphene as a High-Capacity Anode Material for Na- and Ca-Ion Batteries. *ACS Appl. Mater. Interfaces* **2014**, *6*, 1788−1795.

(3) Wang, G.; Shi, G.; Chen, X.; Chen, F.; Yao, R.; Wang, Z. Loading of Free Radicals on the Functional Graphene Combined with Liquid Chromatography−Tandem Mass Spectrometry Screening Method for the Detection of Radical-Scavenging Natural Antioxidants. *Anal. Chim. Acta* **2013**, *802*, 103−112.

(4) Xu, J.; Shen, G. A Flexible Integrated Photodetector System Driven by on-chip Microsupercapacitors. *Nano Energy* **2015**, *13*, 131−139.

(5) Wang, L.; Liu, W.; Zhang, Y.; Zhang, Z.-H.; Tiam Tan, S.; Yi, X.; Wang, G.; Sun, X.; Zhu, H.; Volkan Demir, H. Graphene-based Transparent Conductive Electrodes for GaN-based Light Emitting Diodes: Challenges and Countermeasures. *Nano Energy* **2015**, *12*, 419−436.

(6) Chen, X.; He, Y.; Zhang, Q.; Li, L.; Hu, D.; Yin, T. Fabrication of Sandwich-Structured ZnO/Reduced Graphite Oxide Composite and its Photocatalytic Properties. *J. Mater. Sci.* **2010**, *45*, 953−960.

(7) Al-Enizi, A. M.; Elzatahry, A. A.; Soliman, A. R. I.; Al-Theyab, S. S. Electrospinning Synthesis and Electrocatalytic Performance of Cobalt oxide/Carbon Nanofibers Nanocomposite Based PVA for Fuel Cell Applications. *Int. J. Electrochem. Sc.* **2012**, *7*, 12646−12655.

(8) Xie, L.-J.; Wu, J.-F.; Chen, C.-M.; Zhang, C.-M.; Wan, L.; Wang, J.-L.; Kong, Q.-Q.; Lv, C.-X.; Li, K.-X.; Sun, G.-H. A Novel Asymmetric Supercapacitor with an Activated Carbon Cathode and a Reduced Graphene Oxide−Cobalt Oxide Nanocomposite Anode. *J. Power Sources* **2013**, *242*, 148−156.

(9) Nandapure, B.; Kondawar, S.; Salunkhe, M.; Nandapure, A. Nanostructure Cobalt Oxide Reinforced Conductive and Magnetic Polyaniline Nanocomposites. *J. Compos. Mater.* **2013**, *47* (5), 559−567.

(10) Kumar, R.; Oh, J.-H.; Kim, H.-J.; Jung, J.-H.; Jung, C.-H.; Hong, W. G.; Kim, H. J.; Park, J. Y.; Oh, I.-K. Nanohole-Structured and Palladium-Embedded 3D Porous Graphene for Ultrahigh Hydrogen Storage and CO Oxidation Multi-Functionalities. *ACS Nano* **2015**, DOI: 10.1021/acsnano.5b02337.

(11) Sridhar, V.; Lee, I.; Chun, H.-H.; Park, H. Microwave Synthesis of Nitrogen-Doped Carbon Nanotubes Anchored on Graphene Substrates. *Carbon* **2015**, *87*, 186−192.

(12) Sridhar, V.; Chun, H.-H.; Park, H. 3D Functional Hetero-nanostructures of Vertically Anchored Metal oxide Nanowire Arrays on Porous Graphene Substrates. *Carbon* **2014**, *79*, 330−336.

(13) Parada, C.; Morán, E. Microwave-Assisted Synthesis and Magnetic Study of Nanosized Ni/NiO Materials. *Chem. Mater.* **2006**, *18*, 2719−2725.

(14) Hu, X.; Yu, J. C. High-Yield Synthesis of Nickel and Nickel Phosphide Nanowires via Microwave-Assisted Processes. *Chem. Mater.* **2008**, *20*, 6743−6749.

(15) Xu, C.; Tian, Z.; Shen, P.; Jiang, S. P. Oxide (CeO_2, NiO, Co_3O_4 and Mn_3O_4)-Promoted Pd/C Electrocatalysts for Alcohol Electro-oxidation in Alkaline Media. *Electrochim. Acta* **2008**, *53*, 2610−2618.

(16) Zhang, Z.; Zou, R.; Song, G.; Yu, L.; Chen, Z.; Hu, J. Highly Aligned SnO_2 Nanorods on Graphene Sheets for Gas Sensors. *J. Mater. Chem.* **2011**, *21*, 17360−17365.

(17) Fei, J.; Cui, Y.; Zhao, J.; Gao, L.; Yang, Y.; Li, J. Large-Scale Preparation of 3D Self-Assembled Iron Hydroxide and Oxide Hierarchical Nanostructures and their Applications for Water Treatment. *J. Mater. Chem.* **2011**, *21*, 11742−11746.

(18) Yan, Z.; Ma, L.; Zhu, Y.; Lahiri, I.; Hahm, M. G.; Liu, Z.; Yang, S.; Xiang, C.; Lu, W.; Peng, Z.; Sun, Z.; Kittrell, C.; Lou, J.; Choi, W.; Ajayan, P. M.; Tour, J. M. Three-Dimensional Metal−Graphene−Nanotube Multifunctional Hybrid Materials. *ACS Nano* **2013**, *7*, 58−64.

(19) Zhang, L. L.; Xiong, Z.; Zhao, X. S. Pillaring Chemically Exfoliated Graphene Oxide with Carbon Nanotubes for Photocatalytic Degradation of Dyes under Visible Light Irradiation. *ACS Nano* **2010**, *4*, 7030−7036.

(20) Yang, Z.-Y.; Zhao, Y.-F.; Xiao, Q.-Q.; Zhang, Y.-X.; Jing, L.; Yan, Y.-M.; Sun, K.-N. Controllable Growth of CNTs on Graphene as High-Performance Electrode Material for Supercapacitors. *ACS Appl. Mater. Interfaces* **2014**, *6*, 8497−8504.

(21) Xu, X.; Li, H.; Zhang, Q.; Hu, H.; Zhao, Z.; Li, J.; Li, J.; Qiao, Y.; Gogotsi, Y. Self-Sensing, Ultralight, and Conductive 3D Graphene/Iron Oxide Aerogel Elastomer Deformable in a Magnetic Field. *ACS Nano* **2015**, *9*, 3969−3977.

(22) Pathak, P.; Gupta, S.; Grosulak, K.; Imahori, H.; Subramanian, V. Nature-Inspired Tree-Like TiO_2 Architecture: A 3D Platform for the Assembly of CdS and Reduced Graphene Oxide for Photo-electrochemical Processes. *J. Phys. Chem. C* **2015**, *119*, 7543−7553.

(23) Gerbec, J. A.; Magana, D.; Washington, A.; Strouse, G. F. Microwave-Enhanced Reaction Rates for Nanoparticle Synthesis. *J. Am. Chem. Soc.* **2005**, *127*, 15791−15800.

(24) Fernández-Merino, M. J.; Guardia, L.; Paredes, J. I.; Villar-Rodil, S.; Solís-Fernández, P.; Martínez-Alonso, A.; Tascón, J. M. D. Vitamin C is an Ideal Substitute for Hydrazine in the Reduction of Graphene Oxide Suspensions. *J. Phys. Chem. C* **2010**, *114*, 6426−6432.

(25) Staudenmaier, L. Verfahren zur Darstellung der Graphitsäure. *Ber. Dtsch. Chem. Ges.* **1898**, *31*, 1481−1487.

(26) Wu, Z.-S.; Yang, S.; Sun, Y.; Parvez, K.; Feng, X.; Müllen, K. 3D Nitrogen-Doped Graphene Aerogel-Supported Fe_3O_4 Nanoparticles as Efficient Electrocatalysts for the Oxygen Reduction Reaction. *J. Am. Chem. Soc.* **2012**, *134*, 9082−9085.

(27) Teng, F.; Yao, W.; Zheng, Y.; Ma, Y.; Xu, T.; Gao, G.; Liang, S.; Teng, Y.; Zhu, Y. Facile Synthesis of Hollow Co_3O_4 Microspheres and its use as a Rapid Responsive CL Sensor of Combustible Gases. *Talanta* **2008**, *76*, 1058−1064.

(28) Kurtulus, F.; Guler, H. A Simple Microwave-Assisted Route to Prepare Black Cobalt, Co_3O_4. *Inorg. Mater.* **2005**, *41*, 483−485.

(29) Park, C. S.; Kim, K. S.; Park, Y. J. Carbon-Sphere/Co_3O_4 Nanocomposite Catalysts for Effective Air Electrode in Li/Air Batteries. *J. Power Sources* **2013**, *244*, 72−79.

(30) Ye, D.; Luo, L.; Ding, Y.; Liu, B.; Liu, X. Fabrication of Co_3O_4 Nanoparticles-Decorated Graphene C for Determination of l-Tryptophan. *Analyst* **2012**, *137*, 2840−2845.

(31) Xia, H.; Feng, J.; Wang, H.; Lai, M. O.; Lu, L. MnO_2 Nanotube and Nanowire Arrays by Electrochemical Deposition for Super-capacitors. *J. Power Sources* **2010**, *195*, 4410−4413.

(32) Wei, W.; Cui, X.; Chen, W.; Ivey, D. G. Phase-Controlled Synthesis of MnO_2 Nanocrystals by Anodic Electrodeposition: Implications for High-Rate Capability Electrochemical Supercapacitors. *J. Phys. Chem. C* **2008**, *112*, 15075−15083.

(33) Dresselhaus, M. S.; Dresselhaus, G.; Jorio, A. Universal Properties and Structure of Carbon Nanotubes. *Annu. Rev. Mater. Res.* **2004**, *34*, 247−278.

(34) Wang, G.; Shen, X.; Horvat, J.; Wang, B.; Liu, H.; Wexler, D.; Yao, J. Hydrothermal Synthesis and Optical, Magnetic, and Super-capacitance Properties of Nanoporous Cobalt Oxide Nanorods. *J. Phys. Chem. C* **2009**, *113*, 4357−4361.

(35) Hadjiev, V. G.; Iliev, M. N.; Vergilov, I. V. The Raman Spectra of Co_3O_4. *J. Phys. C: Solid State* **1988**, *21*, L199.

(36) Ahuja, P.; Sahu, V.; Ujjain, S. K.; Sharma, R. K.; Singh, G. Performance Evaluation of Asymmetric Supercapacitor Based on Cobalt Manganite Modified Graphene Nanoribbons. *Electrochim. Acta* **2014**, *146*, 429−436.

(37) Wang, H.-W.; Hu, Z.-A.; Chang, Y.-Q.; Chen, Y.-L.; Zhang, Z.-Y.; Yang, Y.-Y.; Wu, H.-Y. Preparation of Reduced Graphene Oxide/Cobalt Oxide Composites and Their Enhanced Capacitive Behaviors by Homogeneous Incorporation of Reduced Graphene Oxide Sheets in Cobalt Oxide Matrix. *Mater. Chem. Phys.* **2011**, *130*, 672−679.

DOI: 10.1021/acsami.5b04336
ACS Appl. Mater. Interfaces 2015, 7, 15042−15051

(38) Li, B.; Cao, H.; Shao, J.; Li, G.; Qu, M.; Yin, G. Co_3O_4@ Graphene Composites as Anode Materials for High-Performance Lithium Ion Batteries. *Inorg. Chem.* **2011**, *50*, 1628−1632.
(39) Wang, H.; Gao, Q.; Jiang, L. Facile Approach to Prepare Nickel Cobaltite Nanowire Materials for Supercapacitors. *Small* **2011**, *7*, 2454−2459.
(40) He, G.; Li, J.; Chen, H.; Shi, J.; Sun, X.; Chen, S.; Wang, X. Hydrothermal Preparation of Co_3O_4@Graphene Nanocomposite for Supercapacitor with Enhanced Capacitive Performance. *Mater. Lett.* **2012**, *82*, 61−63.
(41) Huang, S.; Jin, Y.; Jia, M. Preparation of Graphene/Co_3O_4 Composites by Hydrothermal Method and Their Electrochemical Properties. *Electrochim. Acta* **2013**, *95*, 139−145.
(42) Li, Q.; Hu, X.; Yang, Q.; Yan, Z.; Kang, L.; Lei, Z.; Yang, Z.; Liu, Z. Electrocapacitive Performance of Graphene/Co_3O_4 Hybrid Material Prepared by a Nanosheet Assembly Route. *Electrochim. Acta* **2014**, *119*, 184−191.
(43) Xiang, C.; Li, M.; Zhi, M.; Manivannan, A.; Wu, N. A Reduced Graphene Oxide/Co_3O_4 Composite for Supercapacitor Electrode. *J. Power Sources* **2013**, *226*, 65−70.
(44) Zhang, D.; Zou, W. Decorating Reduced Graphene Oxide with Co_3O_4 Hollow Spheres and their Application in Supercapacitor Materials. *Curr. Appl. Phys.* **2013**, *13*, 1796−1800.
(45) Ujjain, S. K.; Singh, G.; Sharma, R. K. Co_3O_4@Reduced Graphene Oxide Nanoribbon for High Performance Asymmetric Supercapacitor. *Electrochim. Acta* **2015**, *169*, 276−282.
(46) Zhao, L.; Gao, L. Coating of Multi-walled Carbon Nanotubes with Thick Layers of Tin(IV) Oxide. *Carbon* **2004**, *42*, 1858−1861.
(47) Ruowen, F.; Hanmin, Z.; Yun, L. The Reduction Property of Activated Carbon Fibers. *Carbon* **1993**, *31*, 1089−1094.
(48) Chen, S.; Zeng, H. Improvement of the Reduction Capacity of Activated Carbon Fiber. *Carbon* **2003**, *41*, 1265−1271.
(49) Sattarahmady, N.; Heli, H.; Faramarzi, F. Nickel Oxide Nanotubes−Carbon Microparticles/Nafion Nanocomposite for the Electrooxidation and Sensitive Detection of Metformin. *Talanta* **2010**, *82*, 1126−1135.
(50) Koseoglu, Y.; Kurtulus, F.; Kockar, H.; Guler, H.; Karaagac, O.; Kazan, S.; Aktas, B. Magnetic Characterizations of Cobalt Oxide Nanoparticles. *J. Supercond. Nov. Magn.* **2012**, *25*, 2783−2787.
(51) Banfield, J. F.; Welch, S. A.; Zhang, H.; Ebert, T. T.; Penn, R. L. Aggregation-based Crystal Growth and Microstructure Development in Natural Iron Oxyhydroxide Biomineralization Products. *Science* **2000**, *289* (5480), 751−754.
(52) Alivisatos, A. P. Naturally Aligned Nanocrystals. *Science* **2000**, *289* (5480), 736−737.

DOI: 10.1021/acsami.5b04336
ACS Appl. Mater. Interfaces 2015, 7, 15042−15051